

See discussions, stats, and author profiles for this publication at: <https://www.researchgate.net/publication/309273929>

Flow-Induced Vibrations of Riser Array System

Conference Paper · June 2016

DOI: 10.1115/OMAE2016-54695

CITATIONS

4

READS

320

3 authors, including:



Vaibhav Joshi

Birla Institute of Technology and Science, Pilani - Goa Campus

48 PUBLICATIONS 401 CITATIONS

[SEE PROFILE](#)



Bin Liu

Newcastle University

15 PUBLICATIONS 157 CITATIONS

[SEE PROFILE](#)

OMAE2016-54695

FLOW-INDUCED VIBRATIONS OF RISER ARRAY SYSTEM

Vaibhav Joshi

Keppel-NUS Corporate Lab
National University of Singapore
Singapore

Bin Liu

Department of Mechanical Engineering
National University of Singapore
Singapore

Rajeev K. Jaiman *

Department of Mechanical Engineering
National University of Singapore
Singapore

ABSTRACT

When a riser array system is subjected to a uniform flow, an unstable flow-induced vibration commonly occurs among cylinders, generally called fluid-elastic instability. It can cause long-term or short-term damage to the riser array system. A numerical investigation has been performed in the present study. Generally, flow-induced vibrations include vortex-induced vibration (VIV), wake-induced vibration (WIV), jet switching, turbulent buffeting and fluid-elastic instability. The dynamic interactions among the fluid-induced vibrations, wake interference and proximity interference pose difficulties in the design and operation of the riser array system. The dynamics of a riser array system is very different from that of basic canonical configurations such as side-by-side, tandem and staggered arrangements. In a riser array system, the interferences come from all possible nearby constituent risers. There is a synchronization phenomenon among the cylinders, which may lead to detrimental collisions and short-term failures. It is known that the vortex-induced vibration (VIV) of an isolated circular cylinder is self-limiting. An extensive vibration occurs in the lock-in region within which the frequency of the vortex shedding matches the structural frequency of the immersed structure. In a riser array system, there is a point at which the vibration of cylinder suddenly increases. The vibration of the constituent risers increases without bound with the increment of the free-stream velocity. This free-stream velocity is defined as the critical velocity. The interference not only comes from the inline and cross-flow directions, but also the wake interference from the diagonal upstream risers. In a riser array system, each

riser vibrates independently. However, there is symmetry of frequency spectrum observed about the inline direction along the middle row of the risers.

In this study, the dynamic response of the different risers in the array system is investigated with the help of the amplitude response results from the canonical arrangements (side-by-side and tandem) and wake flow structures. The long top-tensioned riser system can be idealized by two-dimensional elastically mounted cylinders to solve the complex fluid-structure interaction problem. The dynamic response of a typical riser array system has been analyzed at low and high Reynolds number. It is encouraging to see that the results reported in the present investigation can provide useful insight and suggestions in the design and optimization of riser systems to avoid collisions and various long- or short-term failures.

INTRODUCTION

Oil and natural gas are extracted from the earth's crust through the drilling and production risers in the offshore sector. The well head on the sea bed is connected to the surface platform which has the processing facilities with the help of these risers. These risers can go as deep as 10,000 ft to the sea bed depending on the viable location of the natural reservoir. Exposure to the adverse subsea conditions, such as high speed flow current, causes a complex vortex pattern which is observed among the constituent risers. The vortices interact in a very complex manner to induce vibrations. Although in the last few decades, flow-induced vibrations had been reviewed by many authors [1–5], it

*Address all correspondence to this author.

is still challenging for the designers to determine the range of free stream velocities to avoid flow-induced vibrations and collisions, due to the complexities pertaining to mechanism, operating environment, available experimental and numerical analyses.

The vortex dynamics of a riser array system is numerically studied in this paper. To understand the flow-induced vibration of a riser array system, the flow around multiple elastically mounted cylinders can be considered as an idealized model which serves as a generic problem to analyze the offshore risers. The problem is approached through analyzing the basic canonical configurations from the side-by-side to the tandem arrangements. The vortex-induced vibration (VIV) of a circular cylinder mounted elastically has been researched extensively for decades, due to its engineering significance and fundamental value to understand the complexity of fluid-structure interaction. In a cross-flow problem of an isolated circular cylinder, due to asymmetrical vortex shedding, the alternating aerodynamic forces around the cylinder push and pull the cylinder out of its equilibrium position. The resultant structural motion simultaneously increases the complexity and richness of vortex dynamics surrounding the cylinder. This fluid-structure coupling (VIV) produces the maximum vibration amplitude when the reduced velocity is within so-called *lock-in* region [2]. The vortex shedding process in the lock-in region is more complex than the stationary cylinder counterpart. For both stationary and elastically mounted cylinders, the complexity increases further when other cylinders are placed close enough to each other. The interferences are imposed on each other. These interferences in cross flow problem can be broadly classified into two categories, namely proximity interference and wake interference. Numerous research articles regarding the interferences and resultant flow regimes have been published through experimental and numerical investigations of the basic arrangements [6–11]. Proximity effect occurs when two circular cylinders are placed close to each other. The nearby cylinders are completely or partially submerged into the wake of the upstream cylinder. As a result, the vortex formation processes are affected significantly. Proximity interference is particularly significant in a side-by-side arrangement. The wake interference occurs when two cylinders have relatively large distance between them, especially when the downstream cylinder is submerged completely into the wake of the upstream cylinder. The influence on the vortex formation and shedding process of the upstream cylinder is not very strong. Therefore, the wake interference is essentially important in tandem arrangement.

In a riser array system, the unsteady dynamics of these risers is a highly nonlinear superposition of the wake and proximity interference. In such a case, the complexity of the flow field around each cylinder becomes phenomenal and may result in collisions and lead to the structural failure [12]. In a riser array system, the gap flow in the constituent side-by-side arrangement can intermittently cause proximity interference to the shear layers of its nearby risers in transverse direction. There are complex

events of vortex-to-vortex and vortex-to-cylinder interactions in the streamwise direction, causing a synchronization of risers in tandem arrangement. The characteristics of the vibrations of risers in a riser array system are different from VIV of the fundamental arrangements (isolated, tandem, side-by-side and staggered). VIV of the fundamental configurations is self-limiting and only the vibration within the lock-in region is the most intensive. However in the fluid-induced vibration of a riser array system, with the increment of free stream velocity, the vibration amplitude of risers reaches a threshold after which the response of the structure suddenly grows without bound. The corresponding velocity in this circumstance is defined as critical velocity which was first reported in [13] through experimental investigation. It was observed that when the free-stream velocity exceeds the value of critical velocity, the vibration amplitude of the array rapidly increases without bound until it is limited by the tube-tube collisions and nonlinear effects. In the fluid-induced vibration in a riser array system, the interaction of the flow field and the adjacent bluff bodies are the most influential parameters. In the basic arrangements, the lock-in region should be avoided whereas in a riser array, the free-stream velocity should be kept below the critical velocity so as to avoid extensively excited vibrations due to the vibration synchronization among risers.

A typical Tension Leg Platform (TLP) is an example consisting of an array of risers. Usually, a fixed centre to centre distance is maintained between them to avoid any dangerous clashing. Experimental evidence for the fluid-elastic instabilities in such arrangement has been observed. The flow across closely spaced cylinders of equal diameter with motion only in transverse motion was analyzed in [14, 15]. VIV was observed for the complete range of the spacing, while galloping effects were observed for some cases. Analysis of the cylinders with different diameters was performed in [16, 17] with similar characteristics as that of same diameter ones. The relative motion of the riser system with three of the risers with complete motion constraints and one flexibly mounted was studied in [18, 19]. The response of the mounted riser was analyzed with change in the direction of flow. With the fluid medium as air [18], instability was observed which was manifested by the increasing response of the cylinder with the flow velocity. However, with water as the medium [19], high amplitudes were observed and the riser clashed with the mounted supports making the observation more difficult. The experimental work done in [20] dealt with the 3×4 riser array of the Norwegian Fjord system scaled to 1/30 of the prototype. At low currents, high frequency response pertaining to VIV was observed while at high currents, the response was more chaotic and led to collision between the risers. Clashing of risers due to WIV was also observed in [21]. To avoid the clashing of the risers, it is suggested to keep a safe distance of five times the diameter of the risers [22].

In the present work, a similar Tension Leg Platform riser array described above is analyzed. The superimposed phenomenon

of VIV, WIV and proximity interference is rigorously studied. Direct numerical simulation of the array system has been performed to quantify these effects and analyze the response of the different risers. Response of the risers have been analyzed over a range of reduced velocities ($U_r = 2 - 30$). In the following sections, results of the side-by-side and tandem arrangements of circular cylinders will be introduced as a reference for the subsequent analysis of an array of riser system. Following that, detailed analyses of amplitudes, vortex contours and frequency characteristics are discussed. The amplitude response of the riser array is analyzed as a combination of the results from the canonical arrangements (side-by-side and tandem). Eventually, results of riser array system at high Reynolds number of $Re = 10^5$ and reduced velocity of $U_r = 6$ which is typically found in the subsea environment will be discussed for practical applications.

NUMERICAL METHODOLOGY

The Navier-Stokes equations governing an incompressible flow in the arbitrary Lagrangian-Eulerian (ALE) reference frame are considered in the following form

$$\rho^f \left(\frac{\partial \mathbf{u}^f}{\partial t} \Big|_{\hat{x}} + (\mathbf{u}^f - \mathbf{w}) \cdot \nabla \mathbf{u}^f \right) = \nabla \cdot \boldsymbol{\sigma}^f + \mathbf{b}^f \text{ on } \Omega^f(t), \quad (1)$$

$$\nabla \cdot \mathbf{u}^f = 0 \text{ on } \Omega^f(t), \quad (2)$$

where $\mathbf{u}^f = \mathbf{u}^f(\mathbf{x}, t)$ and $\mathbf{w} = \mathbf{w}(\mathbf{x}, t)$ represent the fluid and mesh velocities defined for each spatial point $\mathbf{x} \in \Omega^f(t)$, respectively. In Eq. 1, the partial time derivative with respect to the ALE referential coordinate \hat{x} is kept fixed. The spatial derivatives are taken with respect to the current spatial coordinates denoted by \mathbf{x} . The body force per unit mass applied on the fluid is \mathbf{b}^f and $\boldsymbol{\sigma}^f$ is the Cauchy stress tensor for a Newtonian fluid, written as

$$\boldsymbol{\sigma}^f = -p\mathbf{I} + \mu^f \left(\nabla \mathbf{u}^f + (\nabla \mathbf{u}^f)^T \right). \quad (3)$$

Here, p is pressure in the fluid, \mathbf{I} is the identity tensor and μ^f is the fluid viscosity.

A rigid-body structure immersed in the fluid experiences unsteady vortex-induced forces and consequently may undergo flow-induced vibrations if mounted elastically. The rigid-body motion of the cylinder in the two directions along the Cartesian axes is governed by the following equation:

$$\mathbf{m} \cdot \frac{\partial \mathbf{u}^s}{\partial t} + \mathbf{c} \cdot \mathbf{u}^s + \mathbf{k} \cdot (\varphi^s(\mathbf{z}_0, t) - \mathbf{z}_0) = \mathbf{F}^s + \mathbf{b}^s \text{ on } \Omega^s, \quad (4)$$

where \mathbf{m} , \mathbf{c} and \mathbf{k} denote the mass, damping and stiffness vectors per unit length for the translational degrees of freedom, Ω^s denotes the rigid body, $\mathbf{u}^s(t)$ represents the rigid-body velocity at

time t , \mathbf{F}^s and \mathbf{b}^s are the fluid traction and body forces acting on the rigid body, respectively. φ^s denotes the position vector mapping the initial position \mathbf{z}_0 of the rigid body to its position at time t . The coupled system requires satisfying the no-slip and traction continuity conditions at the fluid-body interface Γ as follows

$$\mathbf{u}^f(\varphi^s(\mathbf{z}_0, t), t) = \mathbf{u}^s(\mathbf{z}_0, t), \quad (5)$$

$$\int_{\varphi(\gamma, t)} \boldsymbol{\sigma}^f(\mathbf{x}, t) \cdot \mathbf{n}^f d\Gamma + \int_{\gamma} \mathbf{F}^s d\Gamma = 0 \quad \forall \gamma \in \Gamma, \quad (6)$$

where \mathbf{n}^f and \mathbf{n}^s are respectively the outer normals to the fluid and the solid. Here, γ is any part of the fluid-body interface Γ and $\varphi(\gamma, t)$ is the corresponding fluid part at time t .

A solver using Petrov-Galerkin finite-element and semi-discrete time stepping has been employed to investigate the interactions of incompressible viscous flow with rigid-body dynamics. To account for fluid-rigid body interaction, a partitioned iterative scheme based on nonlinear interface force correction [23] has been employed for rigid-body coupling and flow-induced vibrations. The temporal discretization of both the fluid and the structural equations is embedded in the generalized- α framework by making use of classical Newmark approximations in time [24]. Throughout this study, the incremental velocity and pressure are computed via the restarted Generalized Minimal Residual (GMRES) solver proposed in [25]. The GMRES uses a diagonal preconditioner and a Krylov space of 30 orthonormal vectors. In the current formulation, we perform Newton-Raphson type iterations to minimize the linearization errors per time step.

PROBLEM DEFINITION

The 3×4 arrangement of the riser array system as shown in Figure 1 is considered for the simulation. The freestream velocity is fixed at a value $u = U$ at the inlet of the domain and the traction vector is set to zero at the outlet boundary. Symmetric boundary conditions are imposed on the side walls corresponding to slip condition and no-slip condition is imposed on the riser walls. Two-dimensional simulations are done for both $Re = 100$ and $Re = 10^5$ with periodic boundary conditions in the third dimension. The length of the domain is set to $L_x = 350D$ and width is set to $L_y = 300D$. The centre of the risers in the first column is at a distance of $L_{Ux} = 154D$ from the inlet boundary and $L_{Dx} = 196D$ from the outlet boundary. All the cylinders are elastically mounted on a spring-damper system with spring constant k and damping coefficient c which is not shown in the figure for clarity. The nomenclature of the risers is done as shown in the figure with riser 5 being the drilling riser. For the study of the VIV-regime ($U_r = 2-8$), the risers are allowed to vibrate in both inline and transverse direction, while for the $U_r = 15-30$, the

inline motion is restricted. This is done to analyze the high reduced velocity regime corresponding to wake-induced vibration, isolating the inline vibration effects.

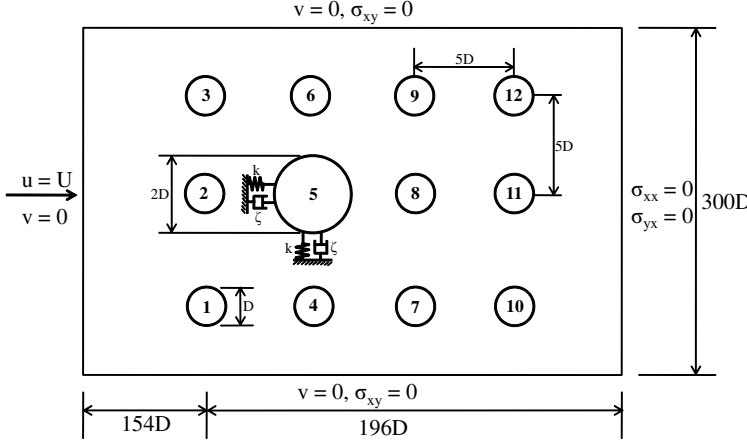


FIGURE 1: Schematic of a 3×4 idealized riser array system with boundary condition details. All the cylinders are elastically mounted. For clarity, only bigger cylinder is shown to be on spring and damper.

Besides the geometric dimensions, the non-dimensional parameters related to the flow-induced vibration are mass ratio (m^*), Reynolds number (Re), reduced velocity (U_r) and damping ratio (ζ) which are defined as:

$$m^* = \frac{M}{m_f}, \quad Re = \frac{\rho^f UD}{\mu^f}, \quad U_r = \frac{U}{f_N D}, \quad \zeta = \frac{c}{2\sqrt{kM}} \quad (7)$$

where $f_N = (1/2\pi)\sqrt{k/M}$ is the dimensional natural frequency, M is the mass per unit length of the cylinder, c and k are the damping and stiffness coefficients respectively of the spring-mass-damper system, U is the freestream velocity, D is the diameter of the cylinder, $m_f = \rho^f \pi D^2/4$ is the mass of displaced fluid by the structure for circular cross-sections, ρ^f is the density of the fluid and μ^f is the dynamic viscosity of the fluid. All the amplitude responses are non-dimensionalized by the small riser diameter D . Moreover, our focus in the high reduced velocity regime $U_r = 10 - 30$ is the effect of wake-induced vibration. Hence, the inline motion of all the risers is restricted in the simulation pertaining to this regime to isolate the transverse vibration.

Mesh convergence studies are done for the side-by-side arrangement case for $Re = 100$ with both the cylinders stationary with centre-to-centre distance of $2.5D$ between them [26]. The

TABLE 1: Mesh convergence analysis for side-by-side configuration at $Re = 100$

Parameters	Mesh 1	Mesh 2	Mesh 3
Number of elements	24,854	50,588	101,956
C_d^{mean}	1.434 (0.4%)	1.429 (0.8%)	1.440
C_L^{mean}	0.180 (3.4%)	0.175 (0.6%)	0.174
St	0.162 (1.8%)	0.162 (1.8%)	0.165

TABLE 2: Validation of the hydrodynamic coefficients for stationary cylinders in side-by-side configuration at $Re = 100$ and centre-to-centre distance of $2.5D$

Literature	C_d^{mean}	C_L^{max}	St
Kang [27]	1.434	0.271	0.164
Carini [28]	1.409	0.262	0.163
Present	1.429	0.272	0.162

TABLE 3: Mesh convergence analysis for tandem configuration at $Re = 100$. (The hydrodynamic coefficients are shown for the downstream cylinder)

Parameters	Mesh 1	Mesh 2	Mesh 3
Number of elements	35,012	71,518	138,390
C_d^{mean}	0.737 (0.14%)	0.731 (0.9%)	0.738
C_L^{rms}	1.059 (0.2%)	1.058 (0.3%)	1.061
St	0.153 (0%)	0.153 (0%)	0.153

mesh convergence results are shown in Table 1. Mesh 2 is chosen to run the simulations. Corresponding validation results for the stationary cylinder case is shown in Table 2.

Table 3 shows the mesh convergence studies for the tandem configuration with both the cylinders stationary at $Re = 100$ and centre-to-centre distance of $5D$ between them. Mesh 2 is chosen to run further simulations. Validation for tandem configuration is done by simulating a case with both cylinders stationary and centre-to-centre distance of $4D$ between them. The comparison is given in Table 4.

The validation for VIV regime at low Reynolds number

TABLE 4: Validation of the hydrodynamic coefficients for stationary cylinders in tandem configuration at $Re = 100$ and centre-to-centre distance = $4D$

Literature	Upstream				Downstream			
	C_d^{mean}	C_d^{rms}	C_L^{rms}	St	C_d^{mean}	C_d^{rms}	C_L^{rms}	St
Sharman et al. [29]	1.2709	0.0158	0.2986	0.1482	0.7044	0.1390	0.9790	0.1482
Present	1.2479	0.0156	0.2957	0.1434	0.6868	0.1370	0.9580	0.1434

($Re = 150$) for a single isolated cylinder is shown and compared with the results of literature [30–32] in Figure 2. The numerical results obtained in present study agree well with those in the literature. Therefore, the numerical algorithm adopted to solve FSI problem in the present study has been successfully verified. The mesh convergence analysis for the turbulent simulation is shown in Table 5. Mesh 2 is adopted for the turbulent simulations of riser array system. It can be interpreted from the mesh convergence analysis that for isolated cylinder case, 45,000 elements within the current domain are approximately sufficient to resolve the hydrodynamic forces around the cylinder for turbulent flows. It can also be seen that by including an additional cylinder within current domain configuration, an additional 10,000 to 12,000 elements is sufficient to provide reasonable hydrodynamic forces around the two cylinders. As a result, in the current riser array system with 12 cylinders, 170,000 elements should be sufficient to generate reasonable numerical results for the cylinder array analysis.

For a practical modeling of turbulence using standard Spalart-Allmaras model, a validation study is performed and the representative results are shown in Figure 3. The time-averaged velocity profile is plotted and compared with the results reported in [33]. The mesh employed for the numerical study of the riser array system consisted of approximately 140,000 nodes with 138,578 six-node wedge elements for $Re = 100$ and 172,390 nodes with 171,190 six-node wedge elements for $Re = 10^5$. For the URANS simulation at $Re = 10^5$, $y^+ \approx 1$ is employed at the boundary layer. Figure 4 shows the full computational domain with a close-up view of the risers.

RESULTS AND DISCUSSION

Before discussion of results of the 3×4 riser array system, observations from the two canonical arrangements (side-by-side and tandem) are reviewed briefly to make the comparisons later.

Side-by-side arrangement

One of the basic arrangements in riser system is side-by-side configuration. In transverse direction, neighboring risers

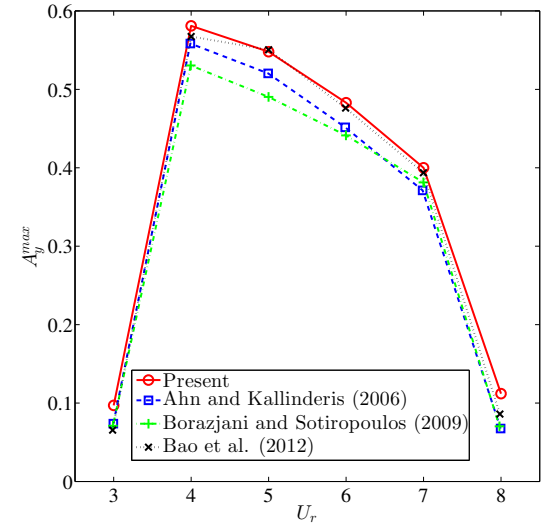


FIGURE 2: Validation of VIV for an isolated circular cylinder at $Re = 150$: Variation of the maximum transverse amplitude with the reduced velocity

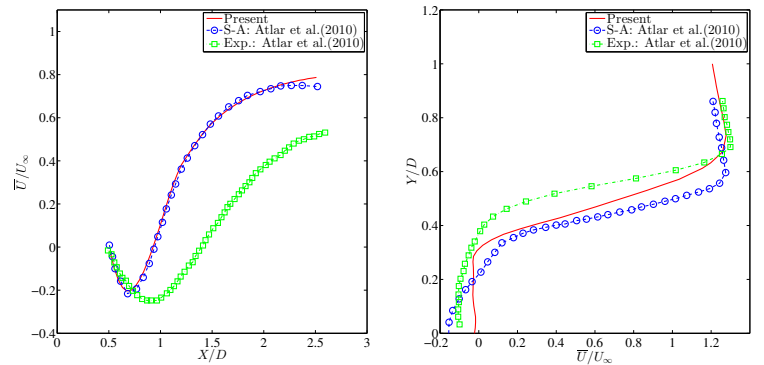


FIGURE 3: Validation of time-averaged velocity profile of an isolated stationary cylinder at $Re = 41300$ (URANS Validation)

TABLE 5: Mesh convergence analysis for an isolated stationary cylinder at $Re = 10^5$

Parameters	Mesh 1	Mesh 2	Mesh 3
Number of elements	25,586	46,442	94,826
Number of elements around cylinder	2,660	3,500	11,620
C_d^{mean}	0.776 (9.3%)	0.709 (0.2%)	0.710
C_L^{rms}	0.656 (21.0%)	0.537 (1.0%)	0.542
St	0.230 (9.1%)	0.245 (3.2%)	0.253

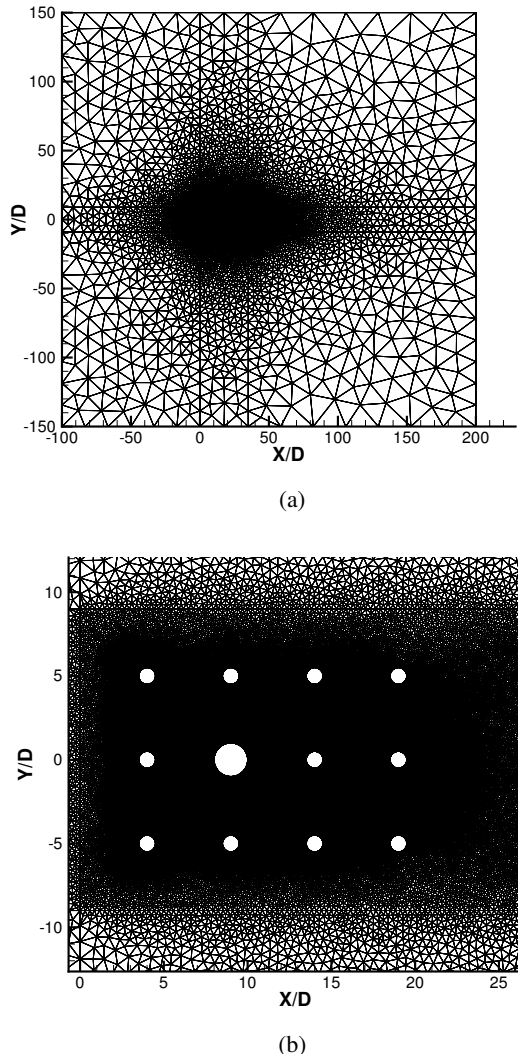


FIGURE 4: Computational mesh employed in the study of riser array system

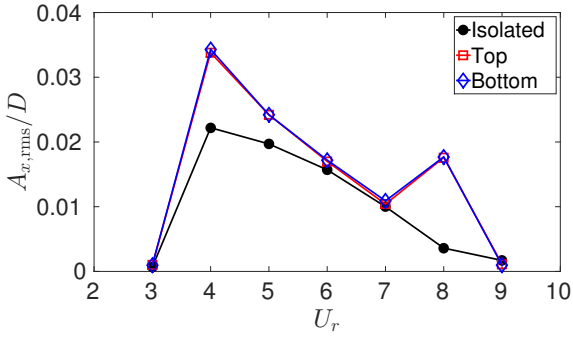
will superimpose interferences on each other. Simulations are done with varying centre to centre distance between the risers in the side-by-side configuration. It is concluded that $5D$ is an appropriate distance to avoid interference between the risers at $Re = 100$. Figure 5 shows the variation of vibration amplitudes for centre to centre distance of $5D$ between the risers. It shows no significant interference between the cylinders. It is also observed from Figure 5(b) that the transverse amplitude of both the risers increase with the increase in reduced velocity in the wake-induced vibration regime ($U_r = 10 - 30$) due to the wake-wake interaction leading to more pronounced transverse amplitude. However, both the risers behave similar to an isolated cylinder in vortex-induced vibration regime ($U_r = 3 - 10$).

Tandem arrangement

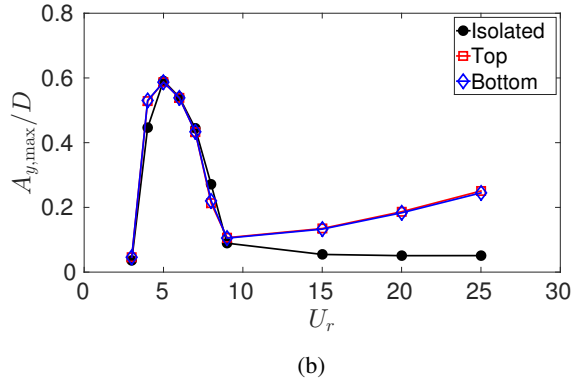
The second basic arrangement of the two elastically mounted cylinders is the tandem configuration with no eccentricity between the centres of the two cylinders. The distance between the two risers is set to $5D$ for the simulations which correspond to the co-shedding regime in which vortex shedding is observed from both the risers with no significant interference of the shed vortices. Numerical simulations pertaining to tandem arrangement at low Re have been performed in [34, 35]. Figure 6 depicts the variation of the vibration amplitudes of the upstream as well as downstream cylinders with reduced velocity. Note that the inline motion is restricted for $U_r = 15, 20, 25$. It is observed that the downstream riser has larger transverse amplitude than the upstream riser in the post lock-in region and beyond. This was also observed in [36] although the upstream cylinder was stationary and the downstream cylinder was allowed motion only in transverse direction. Moreover, the root mean square value of the streamwise amplitude of the downstream riser increases with the reduced velocity which is a peculiar phenomenon.

3×4 riser array system

While the basic configurations (side-by-side and tandem) are assembled, the flow pattern of the flow field is very complex.



(a)



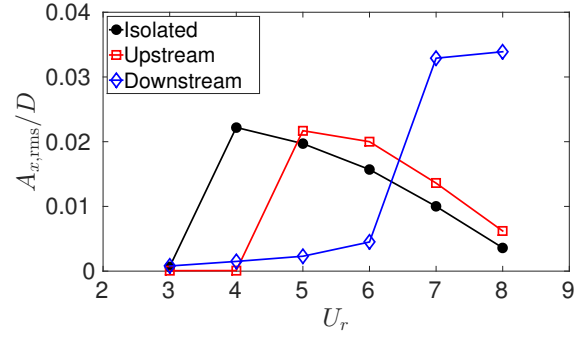
(b)

FIGURE 5: Variation of (a) $A_{x,\text{rms}}/D$ (Inline motion is restricted for $U_r > 9$, hence $A_{x,\text{rms}}/D$ is not defined for the regime) and (b) $A_{y,\text{max}}/D$ of side-by-side arrangement of circular cylinders with varying reduced velocity at $Re = 100$ ($m^* = 2.4, \zeta = 0.001$)

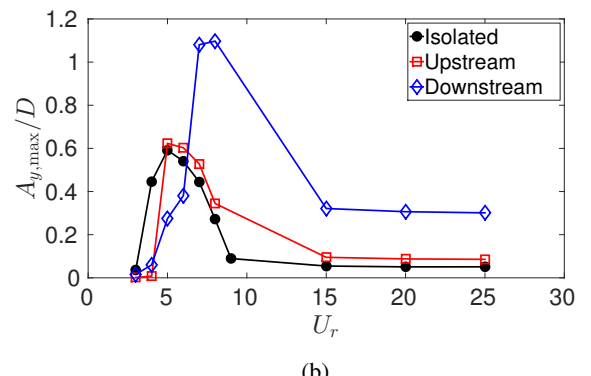
Figure 7 shows the interaction of vortices which are shed from the upstream risers with the downstream risers and their impingement, while Figure 8 shows the contour of the streamline velocity of the riser array system. We can observe an effective wake of the whole system in the figure.

The variation of the vibration amplitudes with the reduced velocity for the array system in the TLP arrangement has been plotted in Figs. 9 and 10. Since the inline motion is restricted for all the risers at high reduced velocity regime, Figure 9 does not contain the range of high U_r . First, we try to analyze the variation of the root mean square of the inline amplitude in $U_r = 2 - 8$ regime (Figure 9). Some of the salient points are:

1. Risers 1, 2 and 3 behave as the upstream riser in the tandem arrangement with heightened inline response of the risers 1 and 3. Riser 2 seems to be shielded and has lower rms value compared to that of risers 1 and 3.
2. As we move towards the downstream risers, we observe the behaviour similar to that of downstream riser in the tandem arrangement, as the $A_{x,\text{rms}}/D$ increases with U_r .
3. Although the $A_{x,\text{rms}}/D$ is less than 20% for the first two



(a)



(b)

FIGURE 6: Variation of (a) $A_{x,\text{rms}}/D$ (Inline motion is restricted for $U_r > 9$, hence $A_{x,\text{rms}}/D$ is not defined for the regime) and (b) $A_{y,\text{max}}/D$ of tandem arrangement of circular cylinders with varying reduced velocity at $Re = 100$ ($m^* = 2.4, \zeta = 0.001$)

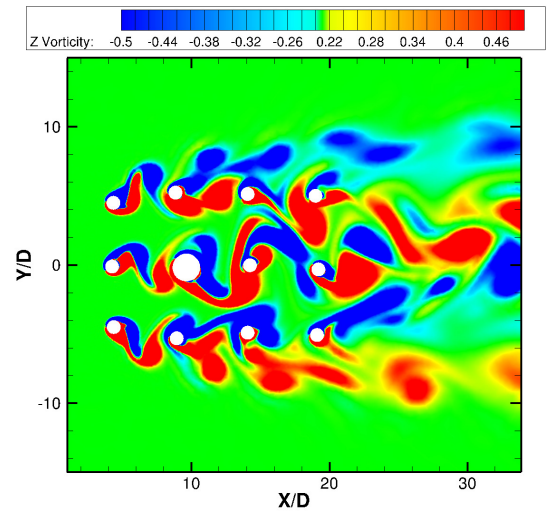


FIGURE 7: Vortex contour plot of the 3×4 riser system at $Re = 100$ ($m^* = 2.4, \zeta = 0.001, U_r = 5$)

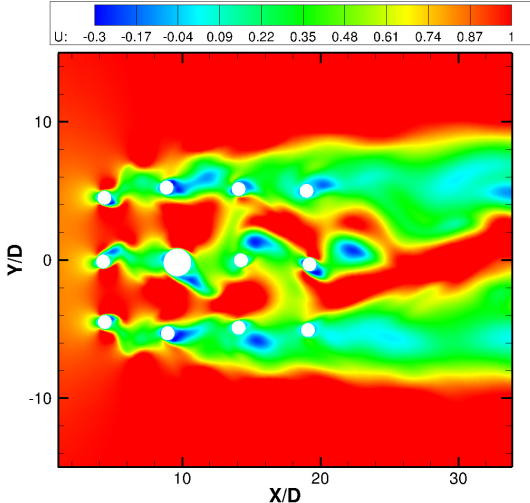


FIGURE 8: Streamwise velocity contour plot of 3×4 riser system at $Re = 100$ ($m^* = 2.4, \zeta = 0.001, U_r = 5$)

columns, it tends to increase without any bound for other risers. Hence, inline motion suppression devices may be needed mainly for the fourth column of risers.

From the transverse amplitude plots (Figure 10), we observe:

1. Risers 1, 2 and 3 behave as upstream riser in tandem arrangement in the $U_r = 2 - 9$ range. However, we observe an increase of the $A_{y,\max}/D$ with U_r for risers 1 and 3 in the $U_r = 15 - 30$ range similar to the observation in the side-by-side arrangement in Figure 5. This can be due to the asymmetrical flow at riser 1 and 3 while the flow is symmetric to riser 2. Riser 2 seems to be shielded from this effect at high U_r .
2. Risers 4 and 6 manifest responses at par with the downstream risers in the tandem arrangement (Figure 6) at low U_r , with the same peculiar behaviour of increase in response at high U_r . Riser 5 is also shielded from the increase in response at high U_r . Comparing riser 1 and 4 (or 3 and 6), the effect of increase in the transverse amplitude due to the incoming wake is observed (tandem-like arrangement).
3. Risers 7 and 9 have similarity to the downstream riser in tandem arrangement with the reduction of amplitude response lower in the post lock-in region ($U_r = 8 - 15$). At high U_r , the same behaviour of side-by-side arrangement is observed. Riser 8 is impinged by a comparatively large vortex from the bigger diameter riser as can be observed in Figure 7. This high energy vortex increases the transverse vibration of the riser. Riser 8 also shows larger amplitude in the VIV regime ($U_r = 5 - 8$) compared to risers on its sides (7 and 9).
4. Riser 11 shows similar behaviour to that of its upstream riser

8. Since, the vortex shed from the riser 8 is smaller compared to the larger vortex of riser 5, it has little effect on the transverse amplitude response of riser 11. Riser 10 and 12 show larger response in the high U_r regime due to the wake of the upstream cylinders.

The frequency amplitude spectrum of the lift coefficient is depicted in Fig. 11. Risers 1, 2 and 3 behave similar to the isolated riser since the dominant frequency is that of an isolated one (≈ 0.17 Hz). Moreover, the spectrum shows symmetry in the response along the middle row of risers. Riser 5 has a different dominant frequency of 0.09 Hz while risers 4 and 6 have combined effects from the wake of first column and the side-by-side wake interference from riser 5. This can be seen in the two frequencies of 0.09 and 0.17 Hz. Analysis of the downstream risers (risers 7-12) show the effect of the frequency of riser 5 as the dominant frequency. Hence, the riser 5 can be considered as the driving element in the low reduced velocity regime ($U_r = 2 - 8$), which regulates the dominant frequencies of the downstream risers. All the downstream risers are synchronized to the frequency of riser 5. Similar behaviour can be seen in the high reduced velocity regime ($U_r = 10 - 30$) where the spectrum for $U_r = 25$ has been plotted in Fig. 12.

In the VIV regime ($U_r = 2 - 7$), the maximum transverse amplitude of the risers was half their diameter, which was also observed in the experiment done in [20]. But, the amplitude increased with higher U_r going to an extent of 1.6 times the riser diameter for the downstream risers (Fig. 10).

At $U_r = 5$, the mean drag coefficient, C_D^{mean} for the riser 5 (drilling riser) was found to be 1.6159 (non-dimensionalized using $2D$ as diameter) while its root mean square lift coefficient, C_L^{rms} was obtained as 0.3867. As we go downstream, the drag coefficient value decreases for each riser in the column. However at $U_r = 25$, the drag increases with the downstream risers from the 3rd to 4th column and so does the lift coefficient which is manifested by the large transverse response of the downstream risers (risers 7-12) shown in Fig. 10.

High Re Computation

For more realistic conditions, the setup is simulated for $Re = 10^5$ with $U_r = 6$ using the Spalart-Allmaras turbulence model. The results showed that the drilling riser had a much higher transverse response and collided with the production riser. Hence, the streamline as well as transverse centre to centre distance between the risers is set to $10D$ for high Re simulations. The maximum transverse amplitude of the drilling riser is observed to be $2.2773D$ which is 1.138 times its diameter. Table 6 depicts the response of all the risers of the array. Figures 13 and 14 show the vortex and streamline velocity contours for the case. We can clearly observe the big-sized vortex being generated at the riser 5 which may impinge on the downstream risers diagonally. The effective wake of the whole riser array system is

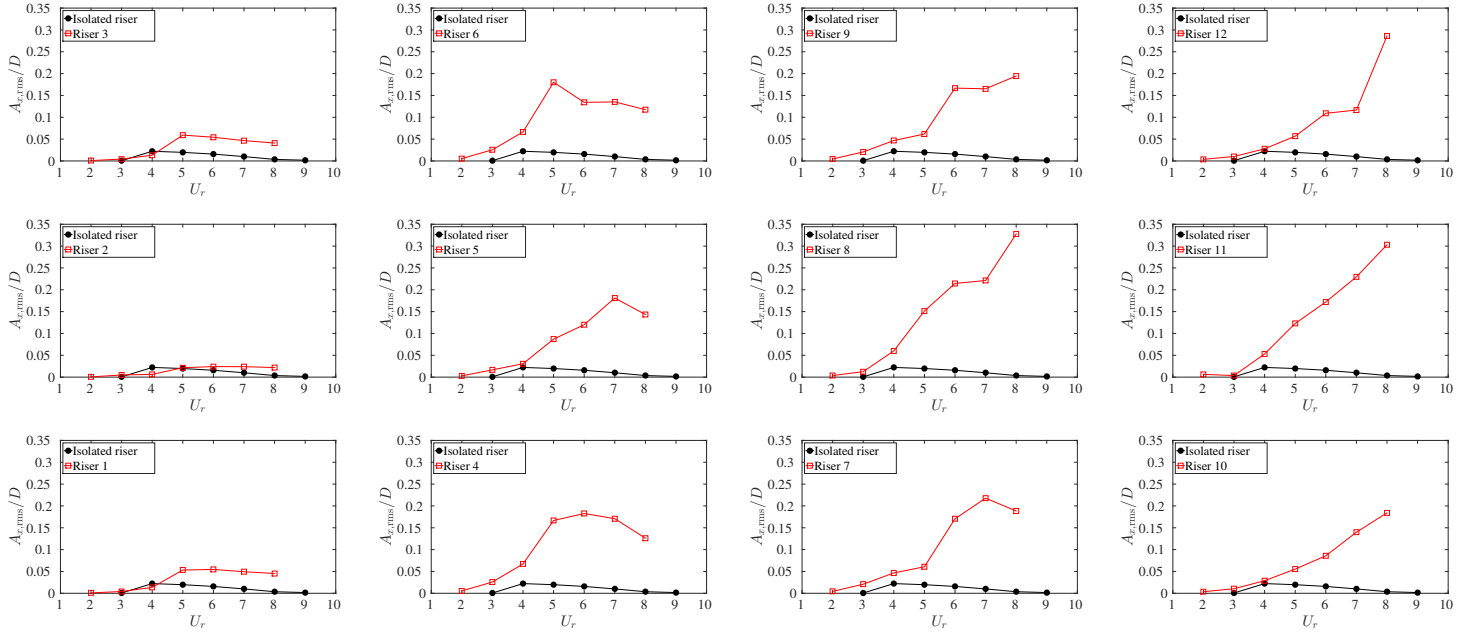


FIGURE 9: Variation of $A_{x,\text{rms}}/D$ of the riser array system with varying reduced velocity at $Re = 100$ ($m^* = 2.4, \zeta = 0.001$). Inline motion is restricted for $U_r > 10$, hence $A_{x,\text{rms}}/D$ is not defined for the regime.

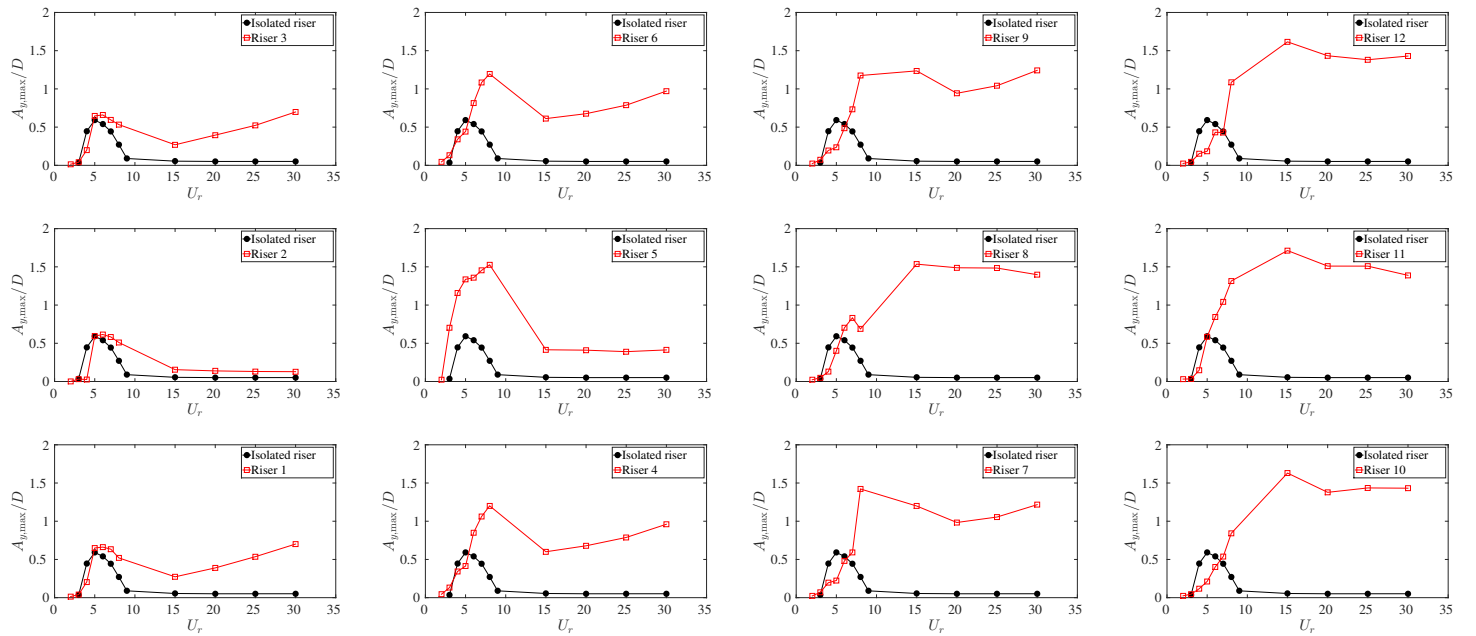


FIGURE 10: Variation of $A_{y,\text{max}}/D$ of the riser array system with varying reduced velocity at $Re = 100$ ($m^* = 2.4, \zeta = 0.001$)

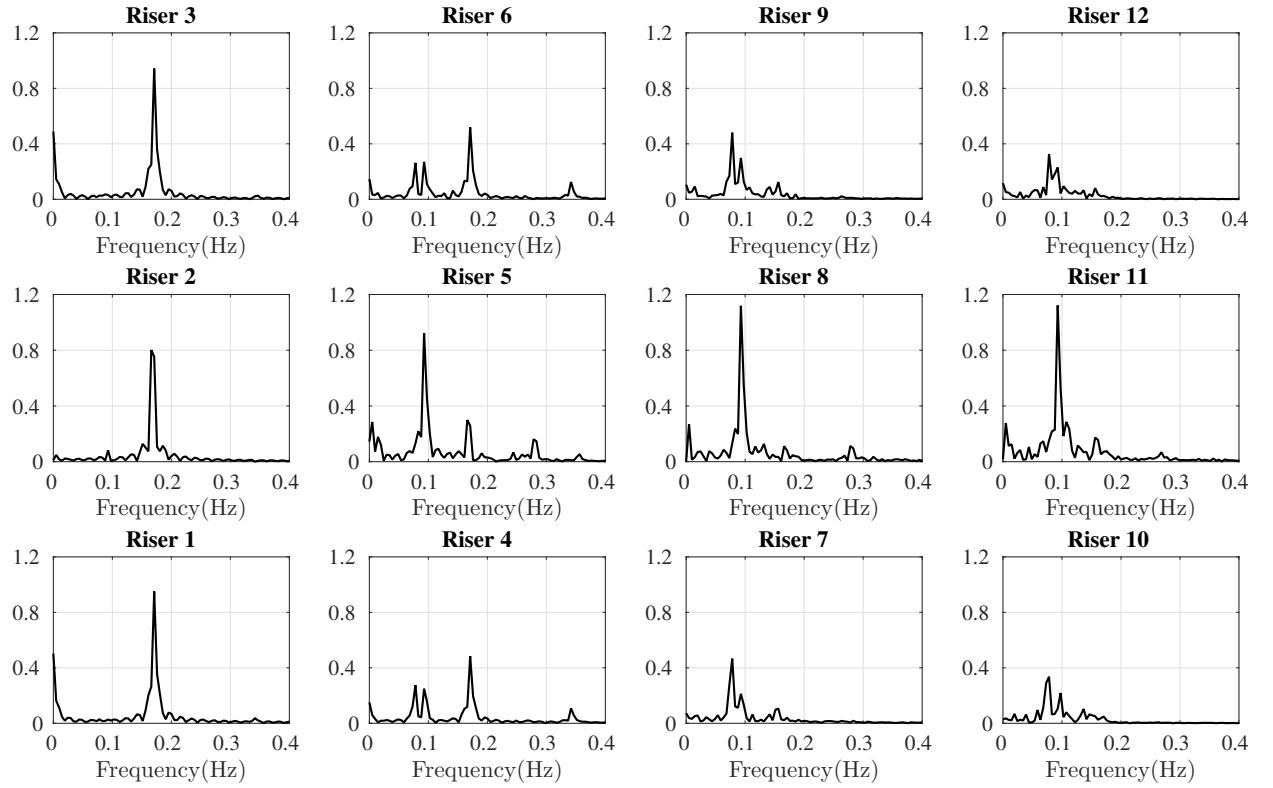


FIGURE 11: Frequency spectrum by FFT at $Re = 100$ ($m^* = 2.4, \zeta = 0.001, U_r = 5$)

observed in the figure.

The mean drag coefficient for the drilling riser is found to be 1.0975 and the root mean square value of the lift coefficient is observed to be 0.3700. For $U_r = 6$ at $Re = 10^5$, similar trend of reduction of the drag coefficient in the risers as one goes downstream is observed as that at $Re = 100$.

CONCLUSIONS AND OUTLOOK

The dynamics of the riser array system is very different from that of the basic arrangements (side-by-side, tandem and staggered). The response of the risers is a combination of wake interference from upstream as well as risers on the sides and diagonals. In the current riser array (center-to-center distance = $5D$), the primary interference is the wake interference. Each riser has different frequency spectrum, however, symmetry of frequency spectrum is observed over inline direction along the middle row in the array system. First, the most influential vibration frequencies (e.g. from riser 5) are manifested by the downstream risers. Therefore, the flow control should be treated primarily on the

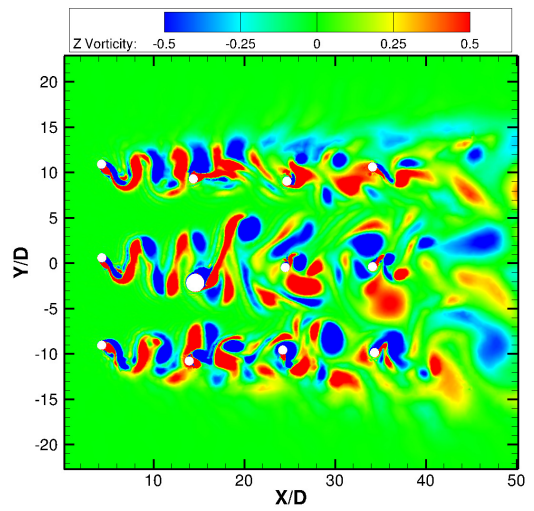


FIGURE 13: Vortex Contour Plot of the 3×4 riser system at $Re = 10^5$ ($m^* = 2.4, \zeta = 0.001, U_r = 6$)

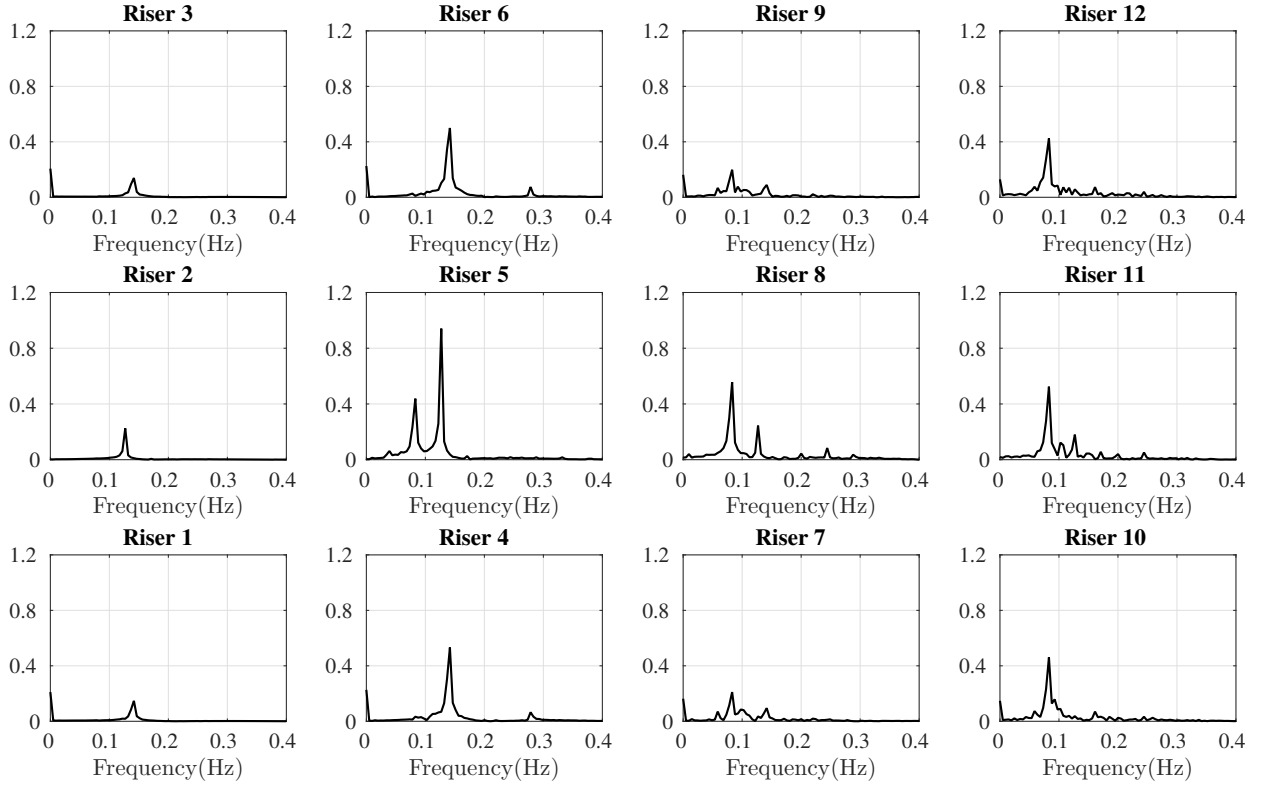


FIGURE 12: Frequency spectrum by FFT at $Re = 100$ ($m^* = 2.4$, $\zeta = 0.001$, $U_r = 25$)

TABLE 6: Inline and transverse response of the riser array system at $Re = 10^5$ ($m^* = 2.4$, $\zeta = 0.001$, $U_r = 6$)

$A_{x,\text{rms},3}/D=0.0654$	$A_{x,\text{rms},6}/D=0.3294$	$A_{x,\text{rms},9}/D=0.3326$	$A_{x,\text{rms},12}/D=0.2394$
$A_{y,\text{max},3}/D=1.0537$	$A_{y,\text{max},6}/D=1.4353$	$A_{y,\text{max},9}/D=1.4534$	$A_{y,\text{max},12}/D=0.9845$
$A_{x,\text{rms},2}/D=0.0489$	$A_{x,\text{rms},5}/D=0.2391$	$A_{x,\text{rms},8}/D=0.1862$	$A_{x,\text{rms},11}/D=0.1466$
$A_{y,\text{max},2}/D=1.1836$	$A_{y,\text{max},5}/D=2.2773$	$A_{y,\text{max},8}/D=1.2215$	$A_{y,\text{max},11}/D=1.0981$
$A_{x,\text{rms},1}/D=0.0660$	$A_{x,\text{rms},4}/D=0.3248$	$A_{x,\text{rms},7}/D=0.2857$	$A_{x,\text{rms},10}/D=0.2710$
$A_{y,\text{max},1}/D=1.0703$	$A_{y,\text{max},4}/D=1.4393$	$A_{y,\text{max},7}/D=1.5783$	$A_{y,\text{max},10}/D=1.1917$

bigger riser so as to damp its vibration strength. Second, the peculiar phenomenon of rise in the response amplitude in the side-by-side case at high U_r is observed. Third, the inline response of the downstream risers tends to grow unbounded with U_r . Hence, suppression of these vibrations should be of importance in the downstream risers. Fourth, due to the wake-induced vibrations and side-by-side effects in the high U_r regime, the transverse amplitude tends to be much higher compared to the VIV regime ($U_r = 4 - 8$). Although the high Re simulations have been carried

out by URANS turbulence modeling, URANS is not able to capture complex vortical flow in the wake region of the cylinders. To obtain more accurate modeling of turbulence, research is towards the Detached Eddy Simulation (DES) which incorporates the benefits of both URANS (near the boundary layer viscous region) and Large Eddy Simulation (LES) in the separated flow wake region.

The future study will focus on the response of the 3D flexible riser array system [37] for a range of reduced velocity corre-

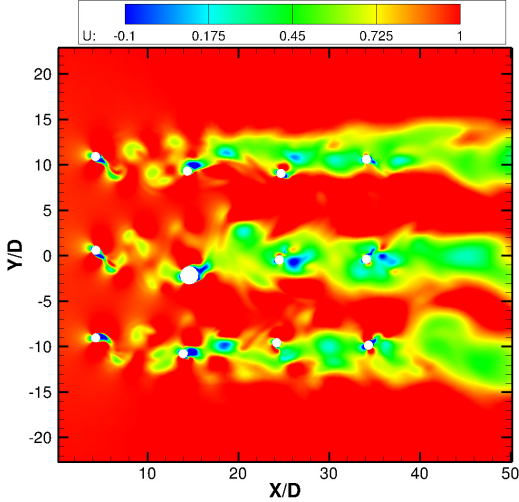


FIGURE 14: Streamwise Velocity Contour Plot of 3×4 riser system at $Re = 10^5$ ($m^* = 2.4$, $\zeta = 0.001$, $U_r = 6$)

sponding to high Reynolds number.

Acknowledgments The first and second authors would like to thank for the financial support from National Research Foundation through Keppel-NUS Corporate Laboratory and Singapore Maritime Institute, respectively. Special thanks to Anis Hussain and Ankit Choudhary of Keppel Offshore & Marine Technology Centre for their industrial inputs. The conclusions put forward reflect the views of the authors alone, and not necessarily those of the institutions.

REFERENCES

- [1] Bearman, P., 2011. “Circular cylinder wakes and vortex-induced vibrations”. *Journal of Fluids and Structures*, **27**, pp. 648–658.
- [2] Sarpkaya, T., 2004. “A critical review of the intrinsic nature of vortex-induced vibrations”. *Journal of Fluids and Structures*, **19**, pp. 389–447.
- [3] Williamson, C., and Govardhan, R., 2004. “Vortex-induced vibrations”. *Annu. Rev. Fluid Mech.*, **36**, pp. 413–455.
- [4] Paidoussis, M., 1981. “Fluid-elastic vibration of cylinder arrays in axial and cross flow: State of the art”. *Journal of Sound and Vibration*, **76**(3), pp. 329–360.
- [5] Weaver, D. S., and Fitzpatrick, J. A., 1988. “A review of cross-flow induced vibrations in heat exchanger tube arrays”. *Journal of Fluids and Structures*, **2**(1), pp. 73–93.
- [6] Sumner, D., 2010. “Two circular cylinders in cross-flow: A review”. *Journal of Fluids and Structures*, **26**(6), pp. 849–899.
- [7] Sumner, D., Price, S. J., and Paidoussis, M. P., 2000. “Flow-pattern identification for two staggered circular cylinders in cross-flow”. *Journal of Fluid Mechanics*, **411**, pp. 263–303.
- [8] Braza, M., Chassaing, P., and Minh, H. H., 1986. “Numerical study and physical analysis of the pressure and velocity fields in the near wake of a circular cylinder”. *Journal of Fluid Mechanics*, **165**, pp. 79–130.
- [9] Mittal, S., Kumar, V., and Raghuvanshi, A., 1997. “Unsteady incompressible flows past two cylinders in tandem and staggered arrangements”. *International Journal for Numerical Methods in Fluids*, **25**(11), pp. 1315–1344.
- [10] Madeleine, C., and Jean-Rene, D., 1991. “Circular cylinder wake configurations: A flow visualization survey”. *American Society of Mechanical Engineers*, **44**(6), pp. 255–305.
- [11] Jaiman, R., Shakib, S., Oakley, O., and Constantinides, Y., 2009. “Fully-coupled fluid-structure interaction for offshore applications”. In ASME Offshore Mechanics and Arctic Engineering OMAE09-79804 CP.
- [12] Paidoussis, M., 1980. “Flow-induced vibrations in nuclear reactors and heat exchangers: Practical experiences and state of knowledge”. *Practical Experiences with Flow-Induced Vibrations*, **829**, p. 832.
- [13] Connors, H., 1970. “Fluid-elastic vibration of tube arrays excited by cross flow”. *Proc. ASME Winter Annual Meet.*, 1970.
- [14] Bokaian, A., and Geoola, F., 1984a. “Wake-induced galloping of two interfering cylinders”. *Journal of Fluid Mechanics*, **146**, pp. 383–415.
- [15] Bokaian, A., and Geoola, F., 1984b. “Proximity-induced galloping of two interfering circular cylinders”. *Journal of Fluid Mechanics*, **146**, pp. 417–449.
- [16] Bokaian, A., and Geoola, F., 1987. “Flow-induced vibrations of marine risers”. *ASCE Journal of Waterway, Port, Coastal and Ocean Engineering*, **113**, pp. 22–38.
- [17] Bokaian, A., and Geoola, F., 1989. “Some observations on the cross flow oscillations of a pair of interfering circular cylinders”. *Aeronautical Journal*, **93**, pp. 66–72.
- [18] Païdoussis, M., Price, S., and Mark, B., 1988. “Current-induced oscillations and instabilities of a multi-tube flexible riser”. *Journal of Fluids and Structures*, **2**, pp. 503–513.
- [19] Price, S., Païdoussis, M., Mark, B., and Mureithi, W., 1989. “Current-induced oscillations and instabilities of a multi-tube flexible riser: Water tunnel experiments”. In Proc. 8th International Conference on Offshore Mechanics and Arctic Engineering, The Hague, Vol. 1, pp. 447–454.
- [20] Huse, E., 1996. “Experimental investigation of deep sea interaction”. In Proc. 28th Offshore Technology Conference, Houston, Vol. 2, pp. 367–372.
- [21] Sagatun, S., Herfjord, K., and Holmås, T., 2002. “Dynamic simulation of marine risers moving relative to each other due to vortex and wake effects”. *Journal of Fluids and Structures*, **16**, pp. 375–390.

- [22] Chakrabarti, S. K., 2004-2005. *Handbook of Offshore Engineering*, Vol. 1-2. Elsevier, Amsterdam; Oxford.
- [23] Jaiman, R., Pillalamarri, N., and Guan, M., 2016. “A stable second-order partitioned iterative scheme for freely vibrating low-mass bluff bodies in a uniform flow”. *Comp. Meth. Appl. Mech. Engrg.*, **301**, pp. 187–215.
- [24] Chung, J., and Hulbert, G., 1993. “A time integration algorithm for structural dynamics with improved numerical dissipation: the generalized- α method”. *J. Appl. Mech.*, **60**, pp. 370–375.
- [25] Saad, Y., and Schultz, M., 1986. “GMRES: A generalized minimal residual algorithm for solving non-symmetric linear systems”. *SIAM Journal on Scientific and Statistical Computing*, **7**.
- [26] Bin, L., and Jaiman, R. K., 2016. “The effect of gap flow on vortex-induced vibration of side-by-side cylinder arrangement”. In ASME Offshore Mechanics and Arctic Engineering OMAE2016-54736.
- [27] Kang, S., 2003. “Characteristics of flow over two circular cylinders in a side-by-side arrangement at low Reynolds numbers”. *Physics of Fluids*, **15**(9), pp. 2486–2498.
- [28] Carini, M., Giannetti, F., and Auteri, F., 2014. “On the origin of the flipflop instability of two side-by-side cylinder wakes”. *Journal of Fluid Mechanics*, **742**(3), pp. 552–576.
- [29] Sharman, B., Lien, F. S., Davidson, L., and Norberg, C., 2005. “Numerical predictions of low Reynolds number flows over two tandem circular cylinders”. *Int. J. Numer. Meth. Fluid*, **47**, pp. 423–447.
- [30] Bao, Y., Huang, C., Zhou, D., Tu, J., and Han, Z., 2012. “Two-degree-of-freedom flow-induced vibrations on isolated and tandem cylinders with varying natural frequency ratios”. *Journal of Fluids and Structures*, **35**, pp. 50–75.
- [31] Ahn, H. T., and Kallinderis, Y., 2006. “Strongly coupled flow/structure interactions with a geometrically conservative ALE scheme on general hybrid meshes”. *Journal of Computational Physics*, **219**(2), pp. 671–696.
- [32] Borazjani, I., and Sotiropoulos, F., 2009. “Vortex-induced vibrations of two cylinders in tandem arrangement in the proximity-wake interference region”. *Journal of fluid mechanics*, **621**, pp. 321–364.
- [33] Atlar, M., Gören, Ö., et al., 2010. “Effect of turbulence modeling on the computation of the near-wake flow of a circular cylinder”. *Ocean Engineering*, **37**(4), pp. 387–399.
- [34] Carmo, B. S., Sherwin, S. J., Bearman, P. W., and Willden, R. H. J., 2011. “Flow-induced vibration of a circular cylinder subjected to wake interference at low reynolds number”. *Journal of Fluids and Structures*, **27**, pp. 503–522.
- [35] Mittal, S., and Kumar, V., 2001. “Flow-induced oscillations of two cylinders in tandem and staggered arrangements”. *Journal of Fluids and Structures*, **15**, pp. 717–736.
- [36] Mysa, R. C., Kaboudian, A., and Jaiman, R. K., 2016. “On the origin of wake-induced vibration in two tandem circular cylinders at low Reynolds number”. *Journal of Fluids and Structures*, **61**, pp. 76–98.
- [37] Springer, M., Jaiman, R., Cosgrove, S., and Constantinides, Y., 2009. “Numerical modeling of vortex-induced vibrations of two flexible risers”. In ASME Offshore Mechanics and Arctic Engineering OMAE09-79801 CP.